Near-field microscopy with a scanning nitrogen-vacancy color center in a diamond nanocrystal: a brief review

A. Drezet[1], Y. Sonnefraud[1], A. Cuche[1,2], O. Mollet[1,3], M. Berthel[1], and S. Huant[1]

(1) Université Grenoble Alpes, Institut NEEL, F-38000 Grenoble,
France and CNRS, Institut NEEL, F-38042 Grenoble, France.
(2) CEMES CNRS UPR 8011, 29 rue J. Marvig, 31055 Toulouse Cedex 4, France.
(3) Laboratoire de Photonique et de Nanostructures (CNRS-LPN), Route de Nozay, 91460 Marcoussis, France.

We review our recent developments of near-field scanning optical microscopy (NSOM) that uses an active tip made of a single fluorescent nanodiamond (ND) grafted onto the apex of a substrate fiber tip. The ND hosting a limited number of nitrogen-vacancy (NV) color centers, such a tip is a scanning quantum source of light. The method for preparing the ND-based tips and their basic properties are summarized. Then we discuss theoretically the concept of spatial resolution that is achievable in this special NSOM configuration and find it to be only limited by the scan height over the imaged system, in contrast with the standard aperture-tip NSOM whose resolution depends critically on both the scan height and aperture diameter. Finally, we describe a scheme we have introduced recently for high-resolution imaging of nanoplasmonic structures with ND-based tips that is capable of approaching the ultimate resolution anticipated by theory.

PACS numbers:

I. MOTIVATION: BEYOND CLASSICAL NEAR-FIELD MICROSCOPY

Since its birth in the early 80's (Pohl et al., 1984), NSOM (Courjon, 2003) became a versatile tool for optical imaging at very high spatial resolution in the nanometer range (Novotny and Hecht, 2006). Yet one fundamental issue with NSOM is the optical resolution offered by a given system. Standard systems based on aperture-NSOM (Pohl et al., 1984) with a hole at the apex of a metal-coated conical tip are fundamentally limited by the size of the optical aperture (Betzig and Chichester, 1993; Gersen et al., 2001; Obermüller et al.; 1995a, Obermüller et al.; 1995b, Drezet et al.; 2002, Drezet et al., 2004a). In order to improve the optical resolution one could ideally use a point-like emitting source.

Recently, inspired by the pioneer work by Michaelis *et al.* (Michaelis et al., 2000) who used a fluorescent single molecule at low temperature as basis for a NSOM, we developed a high-resolution NSOM tip that makes use of an NV center in a diamond nanocrystal as a scanning point-like light source (Cuche et al., 2009a) (see also (Schröder et al., 2011)). In this active tip the 20 nm nanocrystal is glued *in situ* to the apex of an etched optical fiber probe. The NV center acts as a photostable (non blinking, non bleaching) single-photon source working at room temperature (RT) (Beveratos et al., 2002; Sonnefraud et al., 2008). As such, the NV-center based tip proves to be superior to quantum-dot based tips (Chevalier et al., 2005), which suffer from insufficient photostability (Sonnefraud et al., 2006), to insulating-nanoparticle based tips, which, despite remarkable photostability, cannot reach the single-photon emission rate (Cuche et al., 2009b), and to tip-embedded light-emitting-diodes (Hoshino et al., 2012), which are quite involved to fabricate. Therefore, the ND-based NSOM probe opens new avenues for microscopy and quantum optics in the near-field regime.

In this paper we review our contribution to this field and discuss the potentiality of such active-tip based NSOM in terms of spatial resolution. Note that high-resolution apertureless NSOM (Zenhausern et al., 1994; Bachelot et al., 1995) or NSOM based on specially nanostructured passive tips (Mivelle et al., 2014; Eter et al., 2014; Singh et al., 2014) are not covered by the present brief review. In section 2 we describe in detail the fabrication process of such tips and show how to characterize them. We emphasize in particular the quantum properties of the NV emitters and show how to characterize the photon emission statistics of the NV emitters at the NSOM tip apex. In section 3 we show how to use such an active tip for imaging and analyze its optical resolution. The theoretical limit of the optical resolving power is discussed in section 4. and the potentiality of the NV-based NSOM tip in the emerging field of quantum plasmonics is shortly reviewed in section 5. Finally, we present in section 6 some recent results concerning nano-manipulation and displacement of NVs using a NSOM tip.

II. NV CENTER-BASED ACTIVE TIP

Color centers in diamond (Gruber et al., 1997), in particular NV centers, are very promising for the purpose of developing active NSOM. They are room-temperature single-photon emitters (Beveratos et al., 2001; Beveratos et al., 2002), their photostability is well established (Beveratos et al., 2001) and they are hosted by nanocrystals with steadily decreasing sizes thanks to progress in material processing (Chang et al., 2008; Sonnefraud et al., 2008; Boudou et al., 2009; Smith et al., 2009). Early use of NV-center doped diamond nanocrystals in NSOM active tips (Kühn et al., 2001) was, however, limited by the size of the hosting crystal, which was beyond the 50
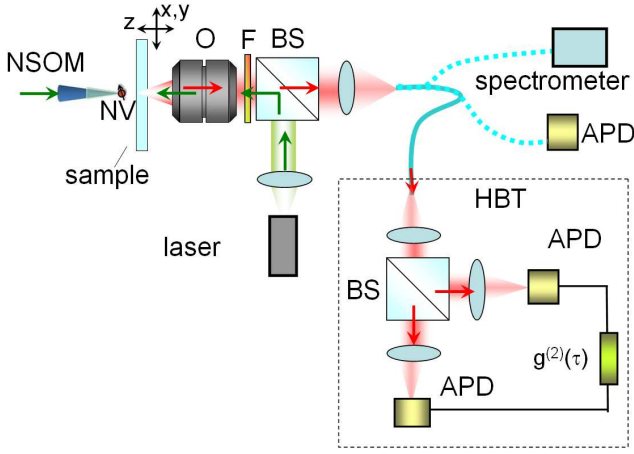
FIG. 1: Scheme of the optical setup used for tip functionalization with a single fluorescent ND; (O= microscope objective, F= optical filters and dichroic mirror, BS= beamsplitter, APD= avalanche photodiode in the single-photon counting mode). The optical excitation from an Ar^+-Kr^+ CW laser is launched from the polymer-coated optical tip and the NV-center fluorescence is collected by a high NA objective, filtered, and injected into a multimode optical fiber. The latter can be connected either to an APD, a spectrometer, or a HBT correlator, which involves a 50/50 BS, two APDs and a time-correlated single-photon counting module (for details see (Cuche et al., 2009)). The latter delivers the second-order time-intensity correlation function $g^{(2)}(\tau)$: see text. Note that a rapid pre-selection of the NDs is usually made prior to the ND grafting: this is achieved by using the setup first in the confocal mode with the excitation being launched to the sample through the microscope objective O directly (green beam on the figure).

nm range, so that the promise of single NV-occupancy, i.e. single-photon emission, was counterbalanced by size excess that prevents positioning with nanometer accuracy. The recent spectacular reduction in size (Chang et al., 2008; Sonnefraud et al., 2008; Boudou et al., 2009; Smith et al., 2009) of fluorescent nanodiamonds (NDs), down to approximately 5 nm (Smith et al., 2009), suggests that such limitation no longer exists and that active optical tips made of an ultra-small (well below 50 nm in size) ND with single NV-occupancy should be possible to achieve.

Our scanning single-photon sources are produced in a single transmission NSOM (Sonnefraud et al. 2006; Sonnefraud et al., 2008) environment. We successively use the optical tip for the imaging and selection of the very ND to be grafted at the tip apex, for controlled attachment of the latter, and subsequent NSOM imaging of test surfaces. A sketch of the optical setup is shown in Fig. 1. After pre-selection of the NDs in the confocal geometry, the NV-center emission is excited with the 488 or 515 nm line of an Ar^+-Kr^+ CW laser that is injected by an uncoated optical tip and is collected into a multimode optical fiber through a microscope objective. The remaining

excitation light is removed by means of a dichroic mirror complemented either by a band-pass filter centered at 607 ± 35 nm for photon counting and imaging or a long-pass filter (> 532 nm) for spectra acquisition of the neutral and negatively-charged NV centers (Dumeige et al., 2004). The collection fiber can be connected either to an avalanche photodiode (APD) for imaging and optical control of the ND manipulation, to a charge-coupled device attached to a spectrometer, or to a Hanbury-Brown and Twiss (HBT) correlator for photon correlation measurements. In the HBT module, a long-pass filter (750 nm) and a diaphragm placed in front of each detector eliminate most of the detrimental optical cross-talk.

The method that we have designed (Cuche et al., 2009a) to trap in a controlled way a well-selected single ND at the optical tip apex is as follows (see Fig. 2). The uncoated optical tip is covered with a thin layer of poly-l-lysine, a polymer able to cover homogenously the tip, including the apex (radius of curvature below 30 nm). In addition, poly-l-lysine is positively charged. This facilitates electrostatic attraction of the NDs, which bear negatively charged carboxylic groups on their surface. This polymer-covered tip is glued on one prong of a tuning-fork (Karrai and Grober, 1995) for shear-force feedback
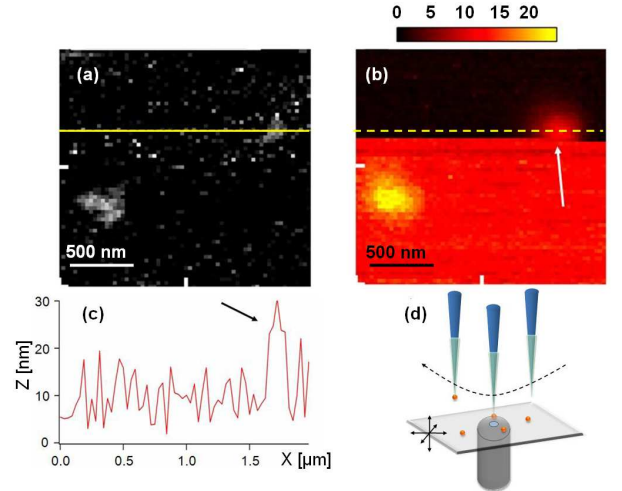

FIG. 2: (a) Topographic and (b) fluorescence NSOM images acquired simultaneously (scale bar in kilo-counts per pixel). Images are recorded pixel by pixel by scanning the sample under the tip from left to right and top to bottom (laser power at the uncoated tip apex: 120 μW; integration time: 80 ms per pixel; scanner speed: 1 μm s^{-1}; image sizes: 64×64 pixel^2). The line cut (c) (horizontal solid line in (b)) gives the ND size (insert) at 20 nm in the present case. The arrow in (b) marks the tip position where the nanodiamond has been attached by the scanning tip. The principle of the complete grafting experiment is sketched in (d) where the NV centers, NSOM tip with polymer, scanning piezo-elements, and microscope objective are all depicted. Images adapted from (Cuche et al., 2009a)

and mounted in the NSOM microscope.

The first step is to image the sample fluorescence to the

far-field by scanning the surface under the optical tip with a very large tip-sample distance of 3 μm. This allows for selecting an interesting area with isolated NDs. In a second step, the tip is brought into the surface near-field by using shear-force regulation. A near-field fluorescence image together with a shear-force topography image are simultaneously recorded at a rather large tip-sample distance of about 50 nm (usual cruise altitudes for NSOM imaging are between 20 and 30 nm) in order to identify an isolated small sized ND with a fluorescence level among the lowest-intensity spots detected in the entire scanned area. This last point is taken as a hint that this very ND presumably hosts a single color center. This essential point can be checked in situ by photon-correlation counting (Sonnefraud et al., 2008), before and after grafting of the ND.

The next step is the ND attachment. This is accomplished "manually" during scanning by strengthening the shear-force feedback (Karrai and Grober, 1995) so as to approach the surface vertically to a distance of around 30 nm with the optical tip facing the desired ND (see Fig. 2(c)). This shear-force strengthening is maintained for typically two scanning lines and then released so as to bring the now functionalized tip back to its initial altitude of 50 nm. Fig. 2 shows an example of a trapping event: It can be seen that the ND trapping manifests itself as a sudden persistent increase in the optical signal. This increase amounts to the emission level of the ND prior to its attachment. Indeed, once the ND has been stuck at the tip apex, the tip not only transmits the excitation laser light, but also produces a background signal due to the attached ND, irrespective of its position above the scanned surface. It is worth noting in Fig. 2(b) that the shear-force feedback has been forced (horizontal dashed line on the fluorescence image) after having made sure that the ND height - 20 nm in the present case - has been measured correctly in the topographic image (full line in Fig. 2(a)). After attachment, the image acquisition is completed and no additional ND is grafted to the tip due to the rather large tip-to-surface distance of around 50 nm (see the sketch of principle in Fig. 2(d)). This is the reason why the 40 nm in-height ND cluster (possibly made of 3 NDs) seen in the lower left quarter in Fig.2 (b) is not trapped by the scanning tip. It is worth noting that an accidental fishing of an additional fluorescent ND would immediately translate into an increase of fluorescence background emanating from the tip: this provides us with a "safety procedure" ensuring that such an accidental fishing would be detected.

Now, the functionalized tip needs further optical characterization since the attached ND was chosen from guesses that it would host a single color-center. To check this important point, we carried out photon-correlation measurements and spectrum acquisition of the functionalized tip after having moved the tip far above the surface (distance of 10 μm), laterally displaced the sample to a ND-free region, and focused the collection objective onto the probe apex.

The second-order time-intensity correlation function is defined in quantum optics and in the stationary regime by

$$g^{(2)}(\tau) = \frac{\langle E^{(-)}(t)E^{(-)}(t+\tau)E^{(+)}(t+\tau)E^{(+)}(t)\rangle}{\langle E^{(-)}(t)E^{(+)}(t)\rangle^2} \quad (1)$$

where $E^{(\pm)}(t)$ are respectively the positive or negative frequency part of the electric field operator associated with the recorded photon stream. For a single-mode photon field in particular, we can introduce the lowering $a(t)$ and raising $a^\dagger(t)$ operators and get

$$g^{(2)}(\tau) = \frac{\langle a^\dagger(t)a^\dagger(t+\tau)a(t+\tau)a(t)\rangle}{\langle a^\dagger(t)a(t)\rangle^2}. \quad (2)$$

In the case of a pure Fock state $|n\rangle$ corresponding to n excitations or quanta in the mode, the previous expression takes the simple form $g^{(2)}(\tau) = n(n-1)/n^2 = 1 - 1/n$. This shows that for $n = 1$, i.e. a single photon, $g^{(2)}(\tau) = 0$. This result can be easily understood if we interpret the $g^{(2)}$ function as a probability function:

$$g^{(2)}(\tau) = \frac{P(t+\tau|t)P(t)}{P(t)^2} = \frac{P(t+\tau|t)}{P(t)} \quad (3)$$

where $P(t)$ is the probability to detect one photon at time t (this probability is independent of t in the stationary regime) and $P(t+\tau|t)$ is the probability to detect a photon at time $t+\tau$ conditioned on the detection of a photon at an earlier time t. For the $|n = 1\rangle$ case we obviously have $P(t + \tau|t) = 0$ since a single photon can only be recorded once.

The second-order correlation function is measured using the HBT correlator shown in Fig. 1. The electric pulses generated by the two single-photon counting detectors are fed into the "start" and "stop" inputs of an electronic counter/timer that both count the number of pulses from each detector and also record the elapsed time between subsequent pulses at the start and stop inputs. The statistical accumulation of coincidence events gives a histogram of the number of events recorded within a particular time interval. Fig. 3(a) shows $g^{(2)}(\tau)$ for the functionalized tip obtained after subtracting the random coincidences caused by the background light (Sonnefraud et al., 2008; Cuche et al., 2009a; Brouri et al., 2000). The correlation function exhibits a clear anti-bunching dip at zero delay with $g^{(2)}(0)$ dropping far below 0.5 (i.e. $g^{(2)}(0) \simeq 0.1$). This unambiguously confirms that a single NV color-center, acting as a single photon nanosource (Cuche et al., 2009a), has been attached at the tip apex. This NV center is an uncharged one as additionally revealed by the optical spectrum of Fig. 3(b) which exhibits the characteristic zero-phonon line of the neutral NV center at 575 nm (Dumeige et al., 2004). We point out that the single photon source does not generate pure Fock states. Indeed, in the considered regime $g^{(2)}(\tau)$ takes the form
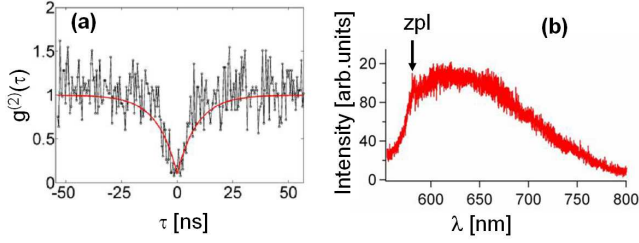
FIG. 3: **(a)** Normalized $g^{(2)}(\tau)$ function for the functionalized tip giving evidence for single NV-center occupancy in the functionalizing ND. The red curve is an exponential fit. **(b)** Photoluminescence spectrum of a functionalized tip (integration time: 180 s). The small peak at 575 nm (indicated by a black arrow) is the zero-phonon line (zpl) of the neutral NV center. Images adapted from (Cuche et al., 2009a)

$$g_{\text{S}}^{(2)}(\tau) = 1 - \frac{1}{N}e^{-(\Gamma+r)\tau} \qquad (4)$$

where N is the number of incoherently excited NV emitters, Γ their typical spontaneous decay constant, and r the excitation rate which, following Fermi rule, is proportional to the laser excitation intensity. From Eq. 4 we deduce $g^{(2)}(0) = 1 - 1/N$, which indeed mimics the pure Fock states for $n = N$. In the presence of an incoherent background taking into account spurious fluorescence due to the sample and the tip itself, Eq. 4 is modified to give $g_{\text{S+B}}^{(2)}(\tau) = 1 - \frac{\rho^2}{N}e^{-(\Gamma+r)\tau}$, where the coefficient $\rho = S/(S + B)$ defines the typical signal intensity (S) to signal + background (B) light intensity ratio. Fig. 3(a) takes into consideration this background light (up to the spurious light coming from the ND itself) by comparing the recorded fluorescence signal before and after the grafting event. The correction ρ allows us to represent directly the histogram $g_{\text{S}}^{(2)}(\tau)$ and to compare it with Eq. 4. The fitting parameters confirm the value $N \simeq 1$ (the small residual value $g^{(2)}(0) \simeq 0.1$ is attributed to the background light coming from the diamond crystal (Cuche et al., 2009a) and from the finite time resolution of the APDs and electronics). The value $(\Gamma + r)^{-1} = 9$ ns gives the red curve in Fig. 3(a). The pumping rate is obtained using the condition $S = \eta r\Gamma/(r+\Gamma)$ with $S \simeq 9$ kHz^{-1} the average photon rate on the APD, and η the total collection-detection efficiency of the whole optical setup including the APDs. Considering the properties of the different elements of the setup we estimate $\eta = 1\%$. This leads to $r^{-1} = 1$ μs and thus to the lifetime $\Gamma^{-1} \simeq 9$ ns. This value concurs with those usually reported (i.e. $\Gamma^{-1} \simeq 10 - 20$ ns) for the considered nanodiamonds (Gruber et al., 1997; Beveratos et al., 2001; Brouri et al., 2000).

We point out that our method is highly reproducible and reliable. We have repeatedly functionalized tips on-demand with a desired number of well-selected NDs in addition to the single ND case described above. For example, as a demonstration of the flexibility of our method, we have been able to successively glue five NDs with a tip, to free all of them at once by knocking the tip on the surface, and to fish them back one by one (Cuche et al., 2010b). Additionnally, in contrast with previous attempts with polymer-free tips which released the embarked nanocrystals within an hour (Cuche et al., 2009c), the ND remains attached at the apex for days so that the functionalized tip can not only be fully characterized, but can also be used in subsequent experiments or imaging.

III. IMAGING AND SPATIAL RESOLUTION

An interesting feature of the scanning single-photon near-field source realized with the above technique is the spatial resolution that it can potentially offer. In order to address this issue we used it to image a test sample made of 250 nm wide and 40 nm thick chromium lines and parabola that have been lithographically patterned on a fused silica cover slip (see Fig. 4(a)). The collection light was spectrally restricted by proper filtering of the NV emission and the scanning height was set at 20 - 30 nm. As can be seen from Fig. 4(b), the optical image clearly reveals the metallic structures as non-transmitting dark lines with a good contrast even though it is recorded with the fluorescence light emitted by a single NV center only. The distinctive bright decorations seen on each side of the chromium structure are possibly due to the finite optical reflectivity of chromium or to modifications of the NV-center dynamical properties (e.g. change in the excited state lifetime or local density of states) when the tip probe approaches the nanostructure edges (Girard et al., 2005). Such effects have been reported for ND emitters located in the vicinity of metal nanostructures (Schietinger et al., 2009).

The chromium parabola in Fig. 4 has been patterned in such a way as to offer a variable gap with the adjacent line. Our aim was to infer a spatial resolution for our setup from its ability of resolving two adjacent similar objects, in agreement with the basic definition of a resolving power, rather than from the lateral extension of the rise in the optical signal. In addition, for this particular line-parabola doublet shown in Fig. 4., a lithography failure brought incidentally the minimum gap to approximately 120 nm (Fig. 4(a)). As seen in Fig. 4(b), this 120 nm gap is resolved in the optical image. This indicates that the spatial resolution is at least in this range, i.e, much better than with the initial uncoated tip which offers resolutions limited to about 400 nm (Sonnefraud et al., 2008). Furthermore, the cross section of the optical intensity profile (see Fig. 4(c)) confirms this finding and indicates that the resolution is at least in the range 70-150 nm.

Moreover, the near-field optical probe reported here acts as a genuine scanning point-like dipole emitter. This contrasts with metal-coated aperture tips which bear
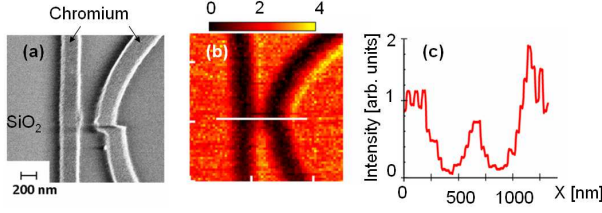
FIG. 4: **(a)** Scanning-electron micrograph of chromium structures patterned on a fused silica cover slip. **(b)** Fluorescence NSOM image acquired simultaneously with the scanning single-photon tip of Figs. 2 and 3 (optical power at 488 nm at the uncoated tip apex: 120 μW, integration time: 100 ms, scan height: h≤ 30 nm, scanner speed: 1 μm s^{-1}, image size: 64×64 pixel^2, scale bar in kilo-counts per pixel). Here, the collected light is restricted by optical filtering to the emission band of the single NV center grafted on the optical tip. **(c)** Cross-cut of the optical recorded signal along the direction indicated by a white line in **(b)** (adapted from (Cuche et al., 2009a))
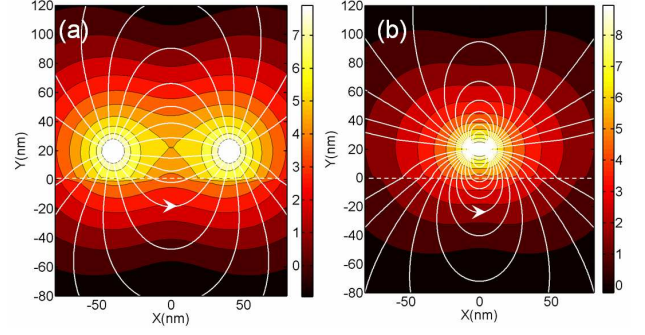

FIG. 5: Electric field generated by an aperture tip **(a)** and a point-like tip **(b)**. The field is calculated with the tip in front of a glass substrate. The vertical distance h between both tips and the glass air interface is $h = 20$ nm. The ring radius is $a = 40$ nm. For each panel the electric field lines and the iso-density curves of the electric energy density $|\mathbf{E}|^2$ (in logarithmic scale) are calculated. The illumination wavelength is $\lambda = 600$ nm (adapted from (Drezet et al., 2011))

a polarization-dependent annular charge density around the apex (Drezet et al., 2004b) that limits the resolution (Drezet et al., 2004a; Drezet et al., 2004b; Betzig and Chichester, 1993; Trautman et al., 1994; van Hulst et al., 2000) and makes such tips mimic a dipolar behavior in the far-field limit only (Obermüller et al., 1995a; Obermüller et al.,1995b; Drezet et al., 2002), not in the near-field. Point-like dipolar emitters do not exhibit such a split-field distribution, so that their potential resolution should thus ultimately depend on the scanning height h only (see next section). Interestingly, the ND-based active tip introduced here could fully exploit this potentiality because the NV quantum emitter is hosted by a matrix of a genuine nanometer extension. This stresses the key role played by height control in future developments. In the present proof-of-principle experiments, we set a safe lower bound to the tip-surface distance at approximately 20-30 nm to avoid too strong friction forces applying to the tip apex (Karrai and Grober, 1995), thereby preventing a too rapid release of the 20-nm sized illuminating ND. We were then able to use our functionalized tips for several days for image acquisition or other measurements. This study clearly shows the potentiality of the NV based NSOM for high resolution imaging. We shall now discuss on a more theoretical basis the ultimate limit of such an active tip and compare it with more usual NSOM aperture tips.

IV. COMPARING A POINT-LIKE EMITTER TO AN APERTURE NSOM TIP

In order to compare theoretically the spatial resolution offered by a classical NSOM aperture tip with the one given by a point-like dipole tip, we first calculate the field generated by both probes. Fig. 5 shows a compari-

son of the electric near-field generated by a ring-like distribution (aperture radius $a = 40$ nm, polarization along the x axis) on the one hand (the method and calculation details are described in (Drezet et al., 2004a; Drezet et al., 2011) and a point-like dipolar source (dipole along the x axis) on the other hand. The comparison is made for a tip facing a glass substrate (permittivity $\epsilon = 2.25$) at a height of $h = 20$ nm. In this configuration the reflected and transmitted fields are calculated with the image method, which is known to give consistent results in the near-field zone (Drezet et al., 2011). The field generated by the ring-like distribution contains both the electric and magnetic contributions but since ka and kh are much smaller than unity we checked that the effect of the magnetic as well as of the propagating terms arising from the field propagator have negligible effects (the same is true for the propagating terms generated by the point-like dipole). However we keep all terms in the calculations for completeness.

In a second stage, we simulate an acquisition scan over an idealized sample. The sample is made of either one or two point-like emitters located at the glass-air interface. To simplify, we also assume that the emitters are fluorescent particles emitting incoherently. The detection of the fluorescent light through the substrate is done with a collection set-up (e.g., a microscope objective with high numerical aperture). More precisely, we consider the photon absorption process by a nanosphere located near $\mathbf{r}$ and containing an isotropic distribution of fluorescent emitters. Following Glauber?s theory (Glauber, 1963) each emitter is excited by the field created by the tip with a probability proportional to $|\mathbf{E}(\mathbf{r}, t)\cdot\mathbf{n}|^2$ where $\mathbf{n}$ is the direction of the transition dipole associated with the point-like fluorescent emitter located at $\mathbf{r}$. Here we suppose a two-step process where the absorption is followed
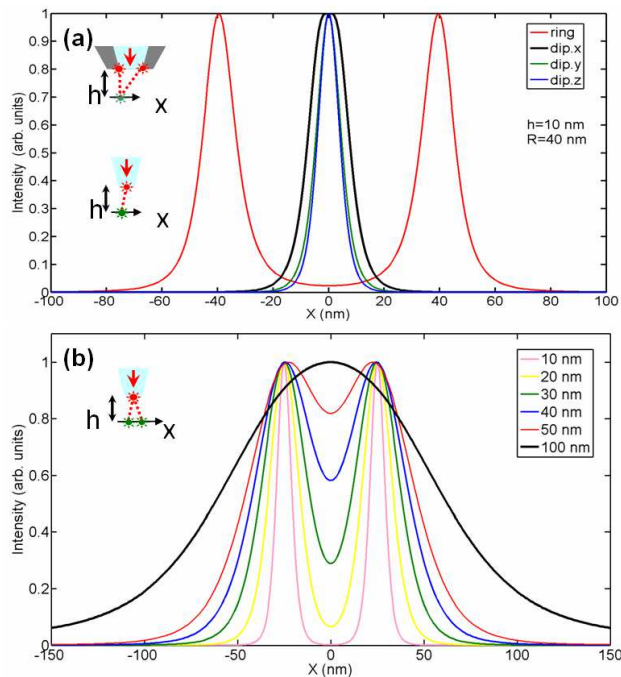
FIG. 6: **(a)** Simulations of the optical image obtained by scanning a fluorescent isotropic emitter at a constant height $h = 10$ nm below the NSOM tip in the ring-like and point-like configurations, respectively (see inserts). The illumination wavelength is $\lambda = 600$ nm. The black curve is the theoretical result obtained for a dipolar point-like source with a dipole oriented along the x direction. Similarly the green and blue curves are the same images for a point-like dipole along the y and z directions, respectively. These curves are compared with the image obtained with an usual aperture NSOM, hole radius: 40 nm (red curve).**(b)** Simulations of the optical image obtained by scanning two fluorescent isotropic emitters separated by a distance $d = 50$ nm (in the scan direction x) at a constant height h below the NSOM point-like probe (i.e., the NV active tip). The different curves correspond to different h going from 10 nm to 100 nm. The probe dipole is along the vertical direction z (adapted from (Drezet et al., 2011))

by a fluorescence emission with probability $\eta(\omega')$ at the emission frequency ω'. After averaging over all possible $\mathbf{n}$ we get a total fluorescence signal for the nanosphere proportional to $\eta(\omega') \cdot |\mathbf{E}(\mathbf{r}, t)|^2$ (Drezet et al., 2004a; Drezet et al., 2004b). Note that in the case of the single-photon tip this picture is very similar to the one used for describing Förster (or fluorescence) resonance energy transfer (FRET) between two molecules (Novotny and Hecht, 2006) (we however neglect the back action of the molecular detectors on the dynamics of the scanning dipole). Therefore the signal recorded at each tip position is supposed to be proportional to the sum of the electric energy density $|\mathbf{E}|^2$ at the location of the point-like fluorescent particles (Girard et al., 2005).

The collection efficiency of the NSOM microscope as used in (Cuche et al., 2009a) is defined by the properties of the high numerical-aperture objective and by the numerical aperture of the multimode fiber which guides the collected light to the detector. We estimate that 62-64% of the 2π solid angle in which light is emitted in the substrate is then collected by the optical setup. This justifies our assumption that essentially all polarisation components of the electric field contribute to the optical signal and therefore that this signal is proportional to $|\mathbf{E}|^2$.

Fig. 6(a) shows the variation of the optical signal during a scan along x for only one isotropic emitter on top of the substrate. The comparison between both tips reveals important optical artifacts with the ring-like NSOM tip due to the finite size of the ring and to the high field intensity in the rim vicinity. These images can easily be interpreted if we consider the fluorescent particle as a test object moving in the near-field of the tips and scanning the emission intensity profile in a plane at constant height h above the apex. The two peaks observed with the usual aperture NSOM are well documented in the literature (Betzig and Chichester, 1993; Gersen et al., 2001; Drezet et al., 2004a) and are reminiscent of the high field available in the rim vicinity. The point-like probe does not show such "doubling" of the imaged structure and this eventually would lead to a simpler interpretation of the optical images.

Having shown that the aperture tip leads to artifacts we consider now the resolving power of the dipole tip. For this purpose we use two scalar fluorescent emitters separated by a distance $d = 50$ nm on the glass substrate. The resolving power will be defined as the ability to distinguish these objects with the NSOM tip. The aperture tip diameter being larger than the gap d we only analyze the resolution of the dipole tip; for more details and comparisons see (Drezet et al., 2004a; Cuche et al., 2009a; Drezet et al., 2004b; Drezet et al., 2011). The results shown in Fig. 6(b) for a dipole orientation along z demonstrate that the resolving power of this kind of microscope is ultimately limited by the height h only. Here, the system offers good resolution even for $h = 50$ nm, i.e. for $h \simeq d$. Only for $h \gtrsim d$ the resolution will be dramatically degraded. These results are actually very general for gaps d much smaller than the wavelength since the near-field of the probe, which is essentially wavelength independent, dominates in this range.

V. QUANTUM PLASMONICS: THE RESOLUTION ISSUE

In this section, we discuss a method we have introduced recently that allows surpassing the resolution limit encountered in section 3 and approaching the theoretical limit discussed in the preceding section.

It is well known that a sub-wavelength object diffracts light into evanescent and propagating waves. It is the evanescent part - the so-called forbidden light - that carries information on the sub-wavelength details of the object. This evanescent contribution plays a key role in experiments targeted at imaging surface-plasmon polari-

tons (SPPs), i.e. electron-photon hybrid states confined at the boundary between a metal and an insulator. As such, SPPs are strongly modified by local changes of their environment at the nanoscale (Barnes et al., 2003; Novotny and Hecht, 2006) and it is therefore critical to find efficient methods to probe the interaction of SPPs with nanostructures. NV-based NSOM tips are particularly adapted for this purpose since they are able to interact locally with the plasmonic environment. Beside this imaging facet, which can be understood in the context of classical Maxwell electromagnetism, it is important to realize that we here enter the realm of quantum optics, i.e., quantum plasmonics. This is because NV centers are single-photon sources. Quantum plasmonics is an emerging field with valuable prospects both on the fundamental science and application agenda. One topic of large impact deals with the coupling of single quantum emitters such as NDs with plasmonic devices. In this context, early and more recent studies have shown that fluorescent quantum emitters can efficiently couple to SPPs when they are located in the vicinity of a metal structure (Drexhage, 1974; Anger et al., 2006; Bharadwaj et al., 2007; Gerber et al., 2007). Moreover, the possibility to generate individual SPPs with single-photon sources opens the door to a wide range of studies such as single-SPP mediated energy transfer (Chang et al., 2006; Akimov et al., 2007; Fedutik et al., 2007; Wei et al., 2009), locally-controlled enhanced fluorescence (Chang et al., 2006; Schietinger et al., 2009), single-SPP interferometry (Kolesov et al., 2009), or SPP quantum interferences (Heeres et al., 2013; Fakonas et al., 2014; Di Martino et al., 2014).

Still, a fundamental understanding together with a tight control in space, energy and polarization within this quantum regime is essential to fully exploit these stimulating promises. Ideally, this requires a deterministic control on the coupling of selected quantum emitters to tailored plasmonic structures (Chang et al., 2006; Girard et al., 2005; Liu et al., 2009). Recently, we made a decisive step forward in this direction by demonstrating deterministic launching of propagative quantum-SPPs at well-defined and freely chosen positions into a nano-structured metal film by using NV-based single photon tips (Cuche et al., 2010a; Mollet et al., 2011; Mollet et al., 2012a; Mollet et al., 2012b). We have been able to demonstrate that the $g^{(2)}(\tau)$ function of the NV sources is fully conserved during the conversion of the evanescent light field to single SPPs and then back to radiative single photons (Mollet et al., 2012a).

For this purpose we used leakage radiation microscopy (LRM) to probe the propagation of SPPs along the metal film. Among the techniques used for imaging SPPs, LRM has emerged as a powerful tool since it gives access in a rather straightforward way to SPPs propagating along the interface between a dielectric and a thin metal film (Hecht et al., 1996; Drezet et al., 2008; Hohenau et al., 2011). In addition, as a far-field technique, LRM can analyze SPP modes both in the direct and Fourier (momen-
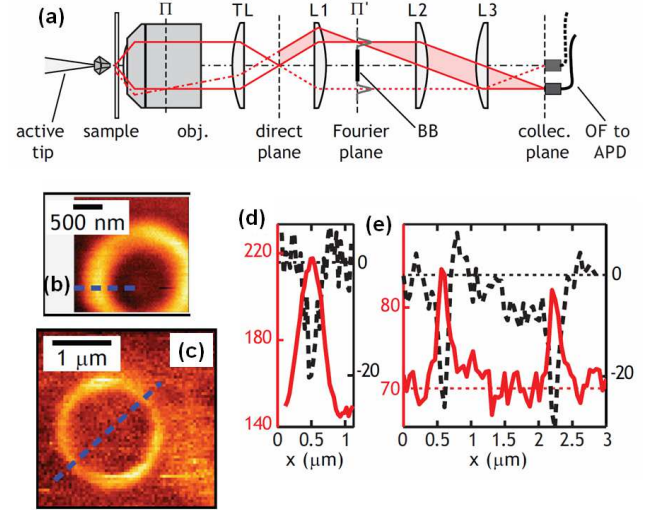

FIG. 7: (a) Layout of the plasmonic microscope: obj.= X100 oil immersion objective of effective numerical aperture $NA = 1.35$; TL= tube lens; L_1, L_2 (removable), L_3= achromatic lenses; BB= beam block; OF= multimode optical fiber; APD= avalanche photodiode. Π' is the back-focal plane of L_1. Π is the objective back-focal plane and is located inside the objective itself. The OF-APD combination can be replaced by a camera (not sketched) aligned with the optical axis for imaging. In this setup, the tip is fixed and the sample is scanned in all three dimensions with nanometer accuracy. The remaining excitation at 515 nm is removed by an optical filter (not shown). A limited number of light rays are indicated for clarity. (b) Direct-space image obtained by scanning the slit under the ND tip. (c) Reconstructed image obtained by mapping the intensity of the SPP circle as function of the slit position under the tip. (d) [respectively (e)] Cross sections along the blue dashed lines in (b) [respectively (c)]. Left scales stand for the optical signal levels, expressed in units of kHz, right scales stand for the topography levels, expressed in nm (adapted from Ref. (Mollet et al., 2012b))

tum) spaces and it has been successfully implemented in various plasmonic systems, both at the classical (Baudrion et al., 2008; Stein et al., 2010; Wang et al., 2011; Bharadwaj et al., 2011; Mollet et al., 2014) and quantum levels (Cuche et al., 2010a; Mollet et al., 2011; Mollet et al., 2012a).

A sketch of LRM coupled to a NSOM is shown in Fig. 7(a). The principle is based on the fact that for thin metal films confined between air and glass, SPPs propagating at the air-metal interface can leak through the film and evolve in the substrate as plane waves emitted at a specific angle Θ_{LRM} (with respect to the optical axis of the microscope). This angle is defined by

$$n_g \sin \Theta_{LRM} = n'_{SPP}(\omega) \qquad (5)$$

where $n_g \simeq 1.5$ is the optical index of glass and $n'_{SPP}(\omega)$ is the real part of the SPP in-plane index at the optical wavelength $\lambda = 2c\pi/\omega$ (Barnes et al., 2003; Drezet et al., 2008). It corresponds to a value larger than the critical angle in glass $\Theta_c = \arcsin(1/n_g)$ ($\Theta_c \simeq 43.2°$ in fused

silica of optical index $n_g \simeq 1.46$). Therefore, leaky SPPs contribute to the 'forbidden' light sector (Novotny and Hecht, 2006). In our setup (Mollet et al., 2012b) we use several lenses for imaging the SPP propagation either in the direct space (conjugated with the air-metal interface of the sample) or in the Fourier space (see Fig. 7(a)). LRM can be combined with a NSOM and Fourier filtering techniques to image SPPs only (Cuche et al., 2010a; Mollet et al., 2011; Mollet et al., 2012a; Mollet et al., 2012b). Our imaging method consists in reconstructing optical images solely from the plasmonic 'forbidden' light collected in the Fourier space. It is demonstrated below by using a point-like ND-based tip that illuminates a thin gold film patterned with a sub-wavelength annular slit. The ND is illuminated through the tip with a $\lambda_{exc.} = 515$ nm laser light. As shown previously (Cuche et al., 2010a; Mollet et al., 2011; Mollet et al., 2012a; Mollet et al., 2012b), the red-orange near-field fluorescence of the NVs launches SPPs into the gold film, whereas the green laser excitation cannot do that because of strong interband absorption in gold in this wavelength range: this is an additional motivation for using a ND tip. This arrangement generates a range of undesired cross-excited nonplasmonic light such as gold fluorescence in addition to the useful plasmonic signal: these photons are filtered using a mask located in the Fourier space (BB in the plane Π' of Fig. 7(a)). In the quantum regime, where only a few photons couple to SPPs, it is crucial to eliminate this nonplasmonic spurious light. The annular slit has a $\simeq 120$ nm rim thickness and $\simeq 1.5$ μm inner diameter. It is patterned by focused-ion beam (FIB) milling in a 30 nm thick gold film. The imaging results are shown in Fig. 7(b-e). It is clear that the reconstructed image in Fig. 7(c) is much better resolved than the direct space image depicted in Fig. 7(b). This is because in the first case the image was recorded by removing all non plasmonic signals (Mollet et al., 2012a; Mollet et al., 2012b), whereas in the second case the image is recorded by collecting photons in the direct space irrespectively of their in-plane momentum. As a matter of fact, the sharpness of the reconstructed image competes with that of the simultaneously acquired topographic image (Mollet et al., 2012b) (not shown here). This is confirmed by the cross sections shown in Figs. 7(d) and (e). In Fig. 7(e), the full width at half maximum of the optical signal is around 130 nm, to compare with 100 nm in the corresponding topographic cross section (Mollet et al., 2012b), whereas in Fig. 7(d) it is as large as 230 nm, compared with 120 nm in the topography. Therefore, reconstructed images from the Fourier-filtered signals made only of high spatial frequencies, i.e. those due to SPPs leaking in the silica substrate, exhibit a four times enhanced spatial resolution of $\simeq 130 - 100 = 30$ nm compared to $\simeq 230 - 120 = 110$ nm obtained in the direct space. This clearly shows the advantage of the reconstruction method concerning resolution. It is worthwhile to note that this 30 nm resolution fits well with the ND size and with the typical distance between tip and surface (Karrai and Grober, 1995) dur-

ing scanning. Therefore, this method offers a resolution that approaches the ultimate spatial resolution achievable with a point-like optical tip as discussed in section 4 (Drezet et al., 2011).

VI. NANO-MANIPULATION OF NV CENTERS USING A NSOM TIP

The possibility to translate precisely a quantum emitter in a structured environment is of tremendous importance for numerous applications, see e.g. (Cuche et al., 2010a; Beams et al., 2013; Schell et al., 2014; Geiselmann et al., 2013; Tisler et al., 2103; Rondin et al., 2014). One application is quantum plasmonics. Recent studies focused on the possibility to locate precisely a quantum emitter near an antenna in order to boost or control its fluorescence/luminescence properties. This is in particular the case for works with an atomic force microscope (AFM) tip used to control precisely the distance between an NV and some gold nanoparticles (Schietinger et al.; 2009) in order to reduce the lifetime of the emitter (an application which could be important for 2D quantum nano-technology). The same group used different approaches based on AFM methods in order to manipulate nano-objects: (i) pushing or (ii) 'fishing'. The first method could be compared to a 'nano-golf' method in which the AFM tip pushes in a gentle way the nanoparticle (Schietinger et al.; 2009) . The second method is
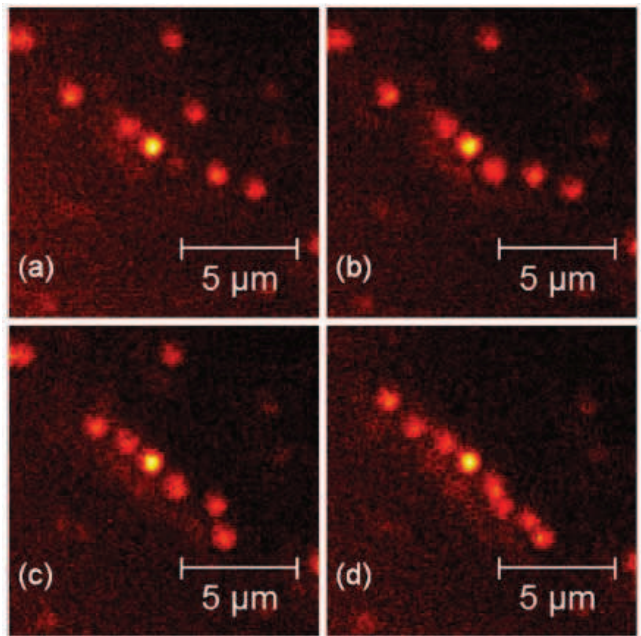
FIG. 8: **(a-d)** An illustration demonstrating how a NSOM tip can be used to align 8 fluorescent diamonds (80 nm diameter) on a glass substrate.

more demanding and requires to be able to pick up a nanoparticle with a tip (using e.g. the NSOM procedure

presented in this manuscript) and then to relax the particle in a controllable way in a given environment (Schell et al., 2011). The clear advantage of the second method is that we can translate the nano-objets over large distances, which is very relevant if these objects are first deposited in a region free of nanostructures.

Due to their interest for applications, we have also investigated the above two methods using NV-based active NSOM tips. Here, we present an example of both approaches. Fig. 8 shows an example of the first procedure. The aim is to translate NV centers contained in 80 nm diameter NDs by using a bare NSOM tip to push and align up to 8 fluorescent NDs. Fig. 8(a-d) show different stages of the experiment involving different number of diamonds. Such an alignment procedure is expected to be of interest in a periodical (plasmonic) system or near an antenna to study the coupling between plasmonic and photonic modes. Fig. 9 shows an example of the second approach (see also (Cuche et al., 2010b) for other demonstrations). Here, the tip with the polymer coating is used to pick up a single fluorescent ND. This diamond is subsequently released at a different position near a colloidal gold nano-prism (10 nm thick and approximately 500 nm side lengths). The method was repeated several times to confirm its reproducibility. The aim of the approach would be to control the lifetime of the emitter near the edges of the triangle.

VII. CONCLUSION

In this article, we have reviewed our contributions to the development of active-tip based NSOM, with a special emphasis on active tips made of a fluorescent ND. In the case of a single NV occupancy in the ND, such a tip forms a genuine scanning single-photon tip. We have discussed the ultimate resolution achieved by such a tip in optical imaging and shown that it is limited by the scan height only, in contrast with standard aperture tips, which are resolution-limited by the aperture size as well. By applying a ND-based tip in SPP launching into a nanostructured gold film and reconstructing images from the Fourier-space SPP signal, we have shown that the scanning plasmonic microscopy achieved this way is able to approach this ultimate resolution. Finally, we demonstrated that the active-based NSOM method is also a versatile tool for moving and positioning precisely NVs in a 2D environment. This represents a promising avenue for future nano-manipulation of quantum emitters in a plasmonic system.

[1] Anger, P., Bharadwaj, P., Novotny, L., 2006. Enhancement and quenching of single-molecule fluorescence. Phys. Rev. Lett. 96, 113002.
[2] Akimov, A. V., Mukherjee, A., Yu, C. L., Chang, D. E., Zibrov, A. S., Hemmer, P. R., Park, H., Lukin, M. D., 2007. Generation of single optical plasmons in metallic nanowires coupled to quantum dots. Nature 450, 402-406.
[3] Bachelot, R., Gleyzes, P., Boccara, A. C., 1995. Near-field optical microscope based on local perturbation of a diffraction spot. Opt. Lett. 20, 1924-1926.
[4] Barnes, W. L., Dereux, A., Ebbesen, T. W., 2003. Surface plasmon subwavelength optics. Nature 424, 824-830.
[5] Baudrion, A.L., de Leon-Perez, F., Mahboub, O., Hohenau, A., Ditlbacher, H., Garcia-Vidal, F.J., Dintinger, J., Ebbesen, T.W., Martin-Moreno, L., Krenn, J.R., 2008. Coupling efficiency of light to surface plasmon polariton for single subwavelength holes in a gold film. Opt. Express 16, 3420-3429.
[6] Beams, R., Smith, D., Johnson, T. W., Oh, S.-H., Novotny, L., Vamivakas, A. N., 2013. Nanoscale fluorescence lifetime imaging of an optical antenna with a single diamond NV center. Nano Lett. 13, 3807-3811.
[7] Betzig, E., Chichester, R. J., 1993. Single molcules observed by near-field scanning Optical microscopy. Science 262, 1422-1425.
[8] Beveratos, A., Brouri, R., Gacoin, T., Poizat, J.-P., Grangier, P., 2001. Nonclassical radiation from diamond nanocrystals. Phys. Rev. A 64, 061802.
[9] Beveratos, A., Kühn, S., Brouri, R., Gacoin, T.,

Poizat, J. P., Grangier, P., 2002. Eur. Phys. J. D 18, 191-196.
[10] Bharadwaj, P., Anger, P., Novotny, L., 2007. Nanoplasmonic enhancement of single-molecule fluorescence. Nanotechnology 18, 044017.
[11] Bharadwaj, P., Bouhelier, A., Novotny, L., 2011. Electrical excitation of surface plasmons. Phys. Rev. Lett. 106, 226802.
[12] Boudou, J.-P., Curmi, P.A., Jelezko, F., Wrachtrup, J., Aubert, P., Sennour, M., Balasubramanian, G., Reuter, R., Thorel, A., Gaffet, E., 2009. High yield fabrication of fluorescent nanodiamonds. Nanotechnology 20, 235602.
[13] Brouri, R., Beveratos, A., Poizat, J. P., Grangier, P., 2000. Photon antibunching in the fluorescence of individual color centers in diamond. Opt. Lett. 25, 1294-1296.
[14] Chang, D. E., Sørensen, A. S., Hemmer, P. R., Lukin, M. D., 2006. Quantum optics with surface plasmons. Phys. Rev. Lett. 97, 053002.
[15] Chang, Y.-R., Lee, H.-Y., Chen, K., Chang, C.-C., Tsai, D.-S., Fu, C.-C., Lim, T.-S., Tzeng, Y.-K., Fang, C.-Y., Han, C.-C., Chang, H.-C., Fann, W., 2008. Mass production and dynamic imaging of fluorescent nanodiamonds. Nature Nanotech. 3, 284-288.
[16] Chevalier, N., Nasse, M. J., Woehl, J. C., Reiss, P., Bleuse, J., Chandezon, F., Huant, S. 2005. CdSe single-nanoparticle based active tips for near-field optical microscopy. Nanotechnology 16, 613-618.
[17] Courjon, D., 2003. Near-field microscopy and near-field optics. Imperial College Press, London.
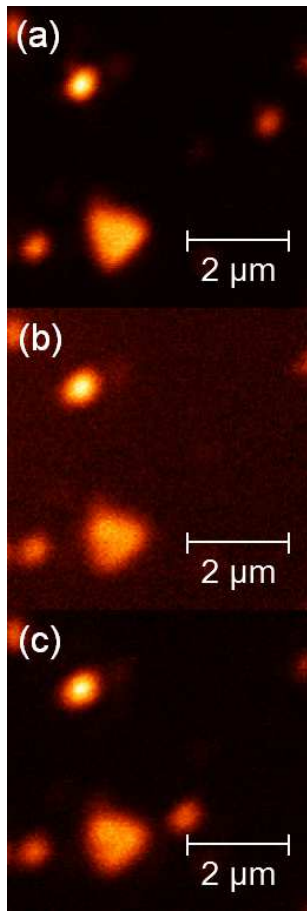[18] Cuche A., Drezet A., Sonnefraud Y., Faklaris O.,

FIG. 9: **(a-c)** An illustration showing how a NSOM tip can be used to first graft and subsequently release a single fluorescent ND (80 nm diameter) on a glass substrate near a plasmonic triangular nano-plate. In (a), the ND is located in the upper right corner of the image. In (b), it has been attached onto the NSOM tip and is no longer visible on the image. In (c), it has been re-deposited on the substrate near the gold triangle in the lower part of the image.

Treussart F., Roch J. F., Huant S., 2009a. Near-field optical microscopy with a nanodiamond-based single-photon tip. Opt. Express 17, 19969-19980.

[19] Cuche, A., Masenelli, B., Ledoux, G., Amans, D., Dujardin, C., Sonnefraud, Y., Melinon, P., Huant, S., 2009b. Fluorescent oxide nanoparticles adapted to active tips for near-field optics. Nanotechnology 20, 015603.

[20] Cuche, A., Sonnefraud, Y., Faklaris, O., Garrot, D., Boudou, J.-P., Sauvage, T., Roch, J.-F., Treussart, F., Huant, S., 2009c. Diamond nanoparticles as photoluminescent nanoprobes for biology and near-field optics. J. Lumin. 129, 1475-1477.

[21] Cuche, A., Mollet, O., Drezet, A., Huant, S., 2010a. "Deterministic" quantum plasmonics. Nano Lett. 10, 4566-4570.

[22] Cuche, A., Drezet, A., Roch, J.-F., Treussart, F., Huant, S., 2010b. Grafting fluorescent nanodiamonds onto optical tips. J. Nanophoton. 4, 043506.

[23] Di Martino, G., Sonnefraud, Y., Tame, M. S., Kna-Cohen, S., Dieleman, F., Özdemir, S. K., Kim, M. S.,

Maier, S. A., 2014. Observation of Quantum Interference in the Plasmonic Hong-Ou-Mandel Effect. Phys. Rev. Applied 1, 034004.

[24] Drexhage, K. H., 1974. Interaction of light with molecular dye lasers. Prog. Opt. 12, 163-232.

[25] Drezet, A., Woehl, J. C., Huant, S., 2002. Diffraction by a small aperture in conical geometry: application to optical tips used in near-field microscopy. Phys. Rev. E 65, 046611.

[26] Drezet A., Nasse M. J., Huant S., Woehl J. C., 2004a. The optical near-field of an aperture tip Europhys. Lett. 66, 41-47.

[27] Drezet, A., Huant, S., Woehl, J. C., 2004b. In situ characterization of optical tips using single fluorescent nanobeads. J. Lumin. 107, 176-181.

[28] Drezet, A., Hohenau, A., Koller, D., Stepanov, A., Ditlbacher, H., Steinberger, B., Aussenegg, F. R., Leitner, A., Krenn, J. R., 2008. Leakage radiation microscopy of surface plasmon polaritons. Mat. Sci. Eng. B 149, 220-229.

[29] Drezet, A., Cuche, A., Huant, S., 2011. Near-field microscopy with a single-photon point-like emitter: Resolution versus the aperture tip? Opt. Commun. 284, 1444-1450.

[30] Dumeige, Y., Treussart, F., Alleaume, R., Gacoin, T., Roch, J.-F., Grangier, P., 2004. Photo-induced creation of nitrogen-related color centers in diamond nanocrystals under femtosecond illumination. J. Lumin. 109, 61-67.

[31] Eter, A. E., Hameed, N. M., Baida, F. I., Salut, R., Filiatre, C., Nedeljkovic, D., Atie, E., Bole, S., Grosjean, T., 2014. Fiber-integrated optical nano-tweezer based on a bowtie-aperture nano-antenna at the apex of a SNOM tip. Opt. Express 22, 10072-10080.

[32] Fakonas, J.S., Lee, H., Kelaita, Y.A., Atwater, H.A., 2014. Two-plasmon quantum interference. Nature. Photon. 8, 317-320.

[33] Fedutik, Y., Temnov, V. V., Schöps, O., Woggon, U., 2007. Exciton-plasmon-photon conversion in plasmonic nanostructures. Phys. Rev. Lett. 99, 136802.

[34] Geiselmann, M., Juan, M. L., Renger, J., Say, J. M., Brown, L. J., Garcia de Abajo, F. J., Koppens, F., Quidant, R., 2013. Three-dimensional optical manipulation of a single electron spin. Nature Nanotech. 8, 175-179.

[35] Gerber, S., Reil, F., Hohenester, U., Schlagenhaufen, T., Krenn, J. R., Leitner, A., 2007. Tailoring light emission properties of fluorophores by coupling to resonance-tuned metallic nanostructures. Phys. Rev. B 75, 073404.

[36] Gersen, H., García-Parajó, M. F., Novotny, L., Veerman, J. A., Kuipers, L., van Hulst, N. F., Near-field effects in single molecule emission. 2001. J. Microscopy 202, 374-378.

[37] Girard, C., Martin, O. J. F., Leveque, G., Colas des Francs, G., Dereux, A., 2005. Generalized bloch equations for optical interactions in confined geometries. Chem. Phys. Lett. 404, 44-48.

[38] Glauber, R. J., 1963. The quantum theory of optical coherence. Phys. Rev. 130, 2529.

[39] Greffet, J. J., Carminati, R., 1997. Image formation in near-field optics. Prog. Surf. Science 56, 133-237.

[40] Gruber, A., Dräbenstedt, A., Tietz, C., Fleury, L., Wrachtrup, J., Von Borczyskowski, C., 1997. Scanning confocal optical microscopy and magnetic resonance on single defect centers. Science 276, 2012-2014.

[41] Hecht, B., Bielefeldt, H., Novotny, L., Inouye, Y., Pohl, D. W., 1996. Local excitation, scattering, and interference of surface plasmons. Phys. Rev. Lett. 77, 1889-1892.

[42] Heeres, R.W., Kouwenhoven, L.P., Zwiller, V., 2013. Quantum interference in plasmonic circuits. Nature Nano. 8, 719-722.

[43] Hohenau, A., Krenn, J. R., Drezet, A., Mollet, O., Huant, S., Genet, C., Stein, B., Ebbesen, T. W., 2011. Surface plasmon leakage radiation microscopy at the diffraction limit. Opt. Express 19, 25749-25762.

[44] Hoshino, K., Gopal, A., Glaz, M. S., Vanden Bout, D. A., Zhang, X., 2012. Nanoscale fluorescence imaging with quantum dot near-field electroluminescence. Appl. Phys. Lett. 101, 043118.

[45] Karrai, K., Grober, R. D., 1995. Piezoelectric tip-sample distance control for near-field optical microscopes. Appl. Phys. Lett. 66, 1842-1844.

[46] Kolesov, R., Grotz, B., Balasubramanian, G., Stöhr, R. J., Nicolet, A. A. L., Hemmer, P. R., Jelezko, F., Wrachtrup, J., 2009. Wave-particle duality of single surface plasmon polaritons. Nature Phys. 5, 470-474.

[47] Kühn, S., Hettich, C., Schmitt, C., Poizat, J.-P., Sandoghdar, V., 2001. Diamond colour centres as a nanoscopic light source for scanning near-field optical microscopy. J. Microsc. 202, 2-6.

[48] Liu, M., Lee, T.-W., Gray, S. K., Guyot-Sionnest, P., Pelton, M., 2009. Excitation of Dark Plasmons in Metal Nanoparticles by a Localized Emitter. Phys. Rev. Lett 102, 107401.

[49] Michaelis J., Hettich C., Mlynek J., Sandoghdar V., 2000. Optical microscopy using a single-molecule light source. Nature 405, 325-328.

[50] Mivelle, M., van Zanten, T. S., Garcia-Parajo, M. F., 2014. Hybrid photonic antennas for subnanometer multicolor localization and nanoimaging of single molecules. Nano Lett. 14, 4895-4900.

[51] Mollet, O., Cuche, A., Drezet, A., Huant, S., 2011. Leakage radiation microscopy of surface plasmons launched by a nanodiamond-based tip. Diam. Relat. Mater. 20, 995-998.

[52] Mollet, O., Huant, S., Dantelle, G., Gacoin, T., Drezet, A., 2012a. Quantum plasmonics: Second-order coherence of surface plasmons launched by quantum emitters into a metallic film. Phys. Rev. B 86, 045401.

[53] Mollet, O., Huant, S., Drezet, A., 2012b. Scanning plasmonic microscopy by image reconstruction from the Fourier space. Opt. Express 20, 28923-28928.

[54] Mollet, O., Bachelier, G., Genet, C., Huant, S., Drezet A., 2014. Plasmonic interferometry: Probing launching dipoles in scanning-probe plasmonics. J. Appl. Phys. 115, 093105.

[55] Novotny, L., Hecht, B., 2006. Principles of Nano-Optics. Cambridge Press, London.

[56] Obermüller, C., Karrai, K., Kolb, G., Abstreiter, G., 1995a.Transmitted radiation through a subwavelength-sized tapered optical fiber tip. Ultramicroscopy 61, 171-177.

[57] Obermüller, C., Karrai, K., 1995b. Far-field characterization of diffracting circular apertures. Appl. Phys. Lett. 67, 3408-3410.

[58] Pohl, D. W., Denk, W., Lanz, M., 1984. Optical stethoscopy: Image recording with resolution $\lambda/20$. Appl. Phys. Lett. 44, 651-653.

[59] Rondin, L., Tetienne, J. P., Hingant, T., Roch, J.-F., Maletinsky, P., Jacques, V., 2014. Magnetometry with nitrogen-vacancy defects in diamond. Rep. Prog. Phys. 77, 056503.

[60] Schell, A. W., Kewes, G., Hanke, T., Leitenstorfer, A., Bratschitsch, R., Benson, O., Aichele, T., 2011. Single defect centers in diamond nanocrystals as quantum probes for plasmonic nanostructures. Opt. Express 19, 7914-7920.

[61] Schell, A. W., Engel, P., Werra, J. F. M., Wolff, C., Busch, K., Benson, O., 2014. Scanning single quantum emitter fluorescence lifetime imaging: quantitative analysis of the local density of photonic states. Nano Lett. 14, 2623-2627.

[62] Schietinger, S., Barth, M., Aichele, T., Benson, O., 2009. Plasmon-Enhanced Single Photon Emission from a Nanoassembled Metal-Diamond Hybrid Structure at Room Temperature. Nano Lett. 9, 1694-1698.

[63] Schröder, T., Schell, A. W., Kewes, G., Aichele, T., Benson, O., 2011. Fiber-integrated diamond-based single photon source. Nano Lett. 11, 198-202.

[64] Singh, A., Calbris., G., van Hulst, N. F., 2014. Vectorial nanoscale mapping of optical antenna fields by molecule dipoles. Nano Lett. 14, 4715-4723.

[65] Smith, B. R., Inglis, D. W., Sandnes, B., Rabeau, J. R., Zvyagin, A. V., Gruber, D., Noble, C. J., Vogel, R., Osawa E., Plakhotnik, T., 2009. Five-Nanometer Diamond with Luminescent Nitrogen-Vacancy Defect Centers. Small 5, 1649-1653.

[66] Sonnefraud, Y., Chevalier, N., Motte, J. F., Huant, S., Reiss, P., Bleuse, J., Chandezon, F., Burnett, M. T., Ding, W., Maier, S. A., 2006. Near-field optical imaging with a CdSe single nanocrystal-based active tip. Opt. Express 14, 10596-10602.

[67] Sonnefraud, Y., Cuche, A., Faklaris, O., Boudou, J. P., Sauvage, T., Roch, J. F., Treussart, F., Huant, S., 2008. Diamond nanocrystals hosting single nitrogen-vacancy color centers sorted by photon-correlation near-field microscopy. Opt. Lett. 33, 611-613

[68] Stein, B., Laluet, J.-Y., Devaux, E., Genet, C., Ebbesen, T.W., 2010. Surface Plasmon Mode Steering and Negative Refraction. Phys. Rev. Lett. 105, 266804.

[69] Tisler, J., Oeckinghaus, T., Stör, R. J., Kolesov, R., Reuter, R., Reinhard, F., Wrachtrup, J., 2013. Single defect center scanning near-field optical microscopy on graphene. Nano Lett. 13, 3152-3156.

[70] Trautman, J. K., Macklin, J. J., Brus, L. E., Betzig, E., 1994. Near-field spectroscopy of single molcules at room-temperature. Nature 369, 40-42.

[71] van Hulst, N. F., Veerman, J.-A., Garcia-Parajo, M. F., Kuipers, L., 2000. Analysis of individual (macro)molecules and proteins using near-field optics. J. Chem. Phys. 112, 7799-7810.

[72] Wang, T., Boer-Duchemin, E., Zhang, Y., Comtet, G., Dujardin, G., 2011. Excitation of propagating surface plasmons with a scanning tunneling microscope. Nanotechnology 22, 175201.

[73] Wei, H., Ratchford, D., Li, X. E., Xu, H., Shih, C.-K., 2009. Propagating surface plasmon induced photon emission from quantum dots. Nano Lett. 9, 4168-4171

[74] Zenhausern, F., Oboyle, M. P., Wickramasinghe, H. K., 1994. Apertureless near-field optical microscope. Appl. Phys. Lett. 65, 1623-1625.